Aerrow: A probe-format graphite calorimeter for absolute dosimetry of high-energy photon beams in the clinical environment

James Renaud[a)]
Medical Physics Unit, McGill University, Montréal, QC, Canada

Arman Sarfehnia
Medical Physics Unit, McGill University, Montréal, QC, Canada
Department of Radiation Oncology, University of Toronto, Toronto, ON, Canada

Julien Bancheri and Jan Seuntjens
Medical Physics Unit, McGill University, Montréal, QC, Canada

(Received 7 February 2017; revised 5 October 2017; accepted for publication 27 October 2017; published 5 December 2017)

Purpose: In this work, the design, operation, initial experimental evaluation, and characterization of a small-scale graphite calorimeter probe — herein referred to as the Aerrow — developed for routine use in the clinical environment, are described. Similar in size and shape to a Farmer type cylindrical ionization chamber, the Aerrow represents the first translation of calorimetry intended for direct use by clinical physicists in the radiotherapy clinic.
Methods: Based on a numerically optimized design obtained in previous work, a functioning Aerrow prototype capable of two independent modes of operation (quasi-adiabatic and isothermal) was constructed in-house. Reference dose measurements were performed using both Aerrow operation modes in a 6 MV photon beam and were directly compared to results obtained with a calibrated reference-class ionization chamber. The Aerrow was then used to quantify the absolute output of five clinical linac-based photon beams (6 MV, 6 MV FFF, 10 MV, 10 MV FFF, and 15 MV; $63.2\% < \%dd(10)\times < 76.3\%$). Linearity, dose rate, and orientation dependences were also investigated.
Results: Compared to an ion chamber-derived dose to water of 76.3 ± 0.7 cGy, the average doses measured using the Aerrow were 75.6 ± 0.7 and 74.7 ± 0.7 cGy/MU for the quasi-adiabatic and isothermal modes, respectively. All photon beam output measurements using the Aerrow in water-equivalent phantom agreed with chamber-based clinical reference dosimetry data within combined standard uncertainties. The linearity of the Aerrow's response was characterized by an adjusted R^2 value of 0.9998 in the dose range of 80 cGy to 470 cGy. For the dose-rate dependence, no statistically significant effects were observed in the range of 0.5 Gy/min to 5.4 Gy/min. A relative photon beam quality dependence of 1.7% was calculated in the range of ^{60}Co to 24 MV ($58.4\% < \%dd(10)\times < 86.8\%$) using Monte Carlo. Finally, the angular dependence (gantry stationary and detector rotated) of the Aerrow's response was found to be insignificant to within ±0.5%.
Conclusions: This work demonstrates the feasibility of using an ion chamber-sized calorimeter as a practical means of measuring absolute dose to water in the radiotherapy clinic. The potential introduction of calorimetry as a mainstream device into the clinical setting is powerful, as this fundamental technique has formed the basis of absorbed dose standards in many countries for decades and could one day form the basis of a new local absorbed dose standard for clinics. © *2017 American Association of Physicists in Medicine* [https://doi.org/10.1002/mp.12669]

Key words: absolute dosimetry, calorimetry, ionization chambers, medical device, reference dosimetry

1. INTRODUCTION

For more than sixty years, calorimeters of various designs have been applied to radiation dosimetry. Today, calorimeters form the basis of primary absorbed dose standards in many countries around the world. These operate on the principle that radiation interacting with matter will result in a measurable temperature rise in the absorbing medium. Even among primary standards, calorimetry is considered the most direct and absolute method of measuring absorbed radiation dose since device calibration can be achieved in terms of quantities with traceable standards (i.e., electrical and temperature), entirely independent of radiation.[1–3] This avoids the need to rely on dosimetric quantities such as $(W/e)_{air}$ (the average energy required to produce an ion pair in dry air) and $(\epsilon(G)_{Fe}^{3+})$ (the product of the molar extinction coefficient and the radiation chemical yield of ferric ions), the knowledge of which are relatively more uncertain than current electrical and temperature-based standards.[1,4] To date, calorimeter designs have primarily been driven by national metrology institutes, whose principal motivation is to achieve the lowest possible measurement uncertainty.[5] Utility and usability of the devices are secondary considerations, and as a result, most calorimeters today are generally both bulky and fragile,

and are operated by only handful of individuals possessing the required specialized equipment and tacit knowledge.[6–11]

In radiotherapy, clinical reference dosimetry of high-energy photon beams is traceable to absorbed dose-to-water standards (most commonly calorimetry). Generally based on calibrating ionization chambers in a standard ^{60}Co field, protocols such as AAPM TG-51 and IAEA TRS-398 detail recommended practices in regard to reference dosimetry.[12–14] The emergence of specialized and nonconformal radiation delivery modalities (MR-linacs, Gammaknife®, Cyberknife®, etc.) incapable of producing a standard reference field (10×10 cm^2) have prompted the development of methodologies to adapt current reference dosimetry traceability to smaller fields.[15] In this approach, a suitable ionization chamber with a conventional calibration traceable to a primary standard is used under nonstandard conditions. Correction factors must then be applied to the chamber readings to account for all the effects (e.g., volume averaging, fluence perturbation, etc.) which cause the detector response to vary between reference and nonreference conditions. Most recently, this correction-based technique has been extended to include the effects due to the presence of a magnetic field.[16]

As a more direct alternative method to realize absorbed dose in nonstandard fields, new graphite and water calorimeters specifically designed to measure dose based on first principles are being developed.[17–19] Oftentimes, these calorimetry systems are also made to be transportable to permit operation at the user's facility.[20–23] Thus, calorimetry-based dose measurements can form the basis of a direct dose calibration of an ionization chamber in the clinically relevant field, or a derivation of their correction factors for those beams. The minimal beam quality and field size dependence of calorimeters also make them useful transfer instruments. Despite their advantages over other dosimetry systems, calorimeters have yet to be incorporated into regular clinical use. Relatively small calorimeters, such as the IMRT calorimeters developed by Duane et al. and Daures et al., rely on vacuum pump systems to achieve pressures of typically less than 10^{-3} Pa in order to minimize the conductive and convective heat transfer inside the calorimeter.[17,18] While incredibly effective at thermally isolating the various constituent bodies of the calorimeter, the time required to establish a partial vacuum, and the challenges associated with maintaining said partial vacuum within a volume of porous graphite, make these relatively expensive solutions impractical for regular clinical use. Any widespread adoption of calorimetry by physicists in the radiotherapy clinic will necessitate a high degree of dependability, robustness, and a relative ease-of-use (i.e., practicality) on the part of the detector.

One aim of this paper is to present the development of a probe-format graphite calorimetry system specifically designed for routine use in the clinical environment (filing no. PCT/CA2013/000523). Originally constructed at McGill University by Renaud et al.[24] the calorimeter, referred to herein as the Aerrow, shares design aspects with graphite calorimeters developed at the Bhabha Atomic Research Centre during the late 1970s,[25] and more recently at the National Physical Laboratory (NPL)[17] and the Laboratoire National Henri Bequerel (LNE-LNHB).[18] Despite these similarities, the Aerrow has not been developed or ever used in a primary standards dosimetry laboratory. Several design and operational aspects of the Aerrow set it apart from standards-level graphite calorimeters. For instance, it's relatively small, probe form factor was purposely chosen to resemble a cylindrical ionization chamber, to ensure minimal disruption to the clinical workflow. Utility-wise, the relatively small sensitive volume will permit it to eventually be tested in nonstandard radiation fields. The Aerrow was also designed to be used directly in water or water-equivalent phantoms, the two mediums most likely encountered in the clinical environment. This is in stark contrast to most primary standards calorimeters, which operate in a reference graphite phantom. Once again, this was done to keep the Aerrow more in line with ionization chambers, but more importantly, measuring directly in water simplifies the dose conversion process and does away with the need for an additional transfer step. In contrast to all other graphite calorimeters, the Aerrow design incorporates aerogel-based material as opposed to a vacuum to achieve thermal isolation from the surrounding environment.[10,11,17–19,25–30] Air gaps have also been successfully used to provide thermal insulation in graphite calorimeter designs (e.g., NPL's portable photon/electron calorimeter), however this design feature necessitates the inclusion of mechanical supports such as expanded polystyrene beads.[23] In this work, aerogel was opted to simplify the assembly process, to maximize the compactness, and to improve the structural robustness of the device. Furthermore, the Aerrow's waterproof holder allows for use in a standard water phantom; a feature not shared by most graphite calorimeters.

Although calorimeters have been used as transfer standards by primary dosimetry calibration laboratories (e.g., Hofmeester and McEwen and Duane),[31,32] this work is the first that has the overarching goal to develop a calorimeter suitable for widespread use by clinicians. Given the state of the calorimetry at the level of the standards labs, it is not inconceivable that such a device could be refined to the point of measuring absorbed dose to water more accurately than currently achievable with ionization chambers, currently the 'gold standard'. Perhaps more importantly, it may serve to increase confidence in dose delivery in small and nonstandard radiation fields (e.g., small and composite fields, or in the presence of an MR-field). In this paper, the design and operating principles of the Aerrow system are presented, and a comparison of the Aerrow's two independent operating modes against a reference-class ionization chamber in a high-energy photon beam is described. The corrections and dose conversion factors necessary to determine absorbed dose to water for high-energy photon beam dosimetry are also discussed. Additionally, a detailing of the Aerrow's relative characterization (linearity, dose-rate dependence, beam quality dependence, and angular dependence) is provided. Note that the Aerrow, while capable in principle of absorbed dose measurement in absolute terms, is not a primary standard. A

primary absorbed dose standard implies an absolute dosimeter embedded in a matrix of exacting metrological practices that is accepted by the community as the measurement against which all other are normalized.

2. METHODS

2.A. Graphite calorimeter

The Aerrow (fourth prototype iteration; MK-IV) is depicted in Fig. 1 by a cross-sectional schematic [Fig. 1(a)] and digitally reconstructed radiograph of a micro-CT scan [Fig. 1(b)]. Similar in size to a 0.6 cm^3 cylindrical ionization chamber [Fig. 1(c)], the Aerrow was originally conceived to determine the absorbed dose to a small sensitive volume, either in a water or solid phantom, in ^{60}Co or high-energy clinical accelerator-based photon beams, down to field sizes of 2×2 cm^2. Unlike an ionization chamber however, the Aerrow was built with the aim of providing an absolute measure of the absorbed dose without the need of a dose calibration coefficient, nor setup-dependent correction factors (e.g., polarity, ion recombination, temperature, pressure, humidity, etc.). The incorporation of an aerogel-based thermal insulator (Pyrogel® 2250, Aspen Aerogels Inc., Northborough, MA, USA) has been the enabling idea behind the development of this device.

The graphite components of the calorimeter (Grade R 4340, SGL Carbon Group, $\rho = 1.72$ g cm^{-3}) are arranged in a nested cylindrical geometry. The 6.1 mm diameter, 10.0 mm long graphite core (i.e., the sensitive volume) is separated from a 0.7 mm thick jacket by a 0.7 mm isotropic layer of Pyrogel insulation. Likewise, a 1.0 mm layer of Pyrogel thermally isolates the jacket from a 1.0 mm thick graphite shield. The mechanical support provided by the solid insulation maintains the constant relative positioning of the graphite components, and allows for regular handling by the user.

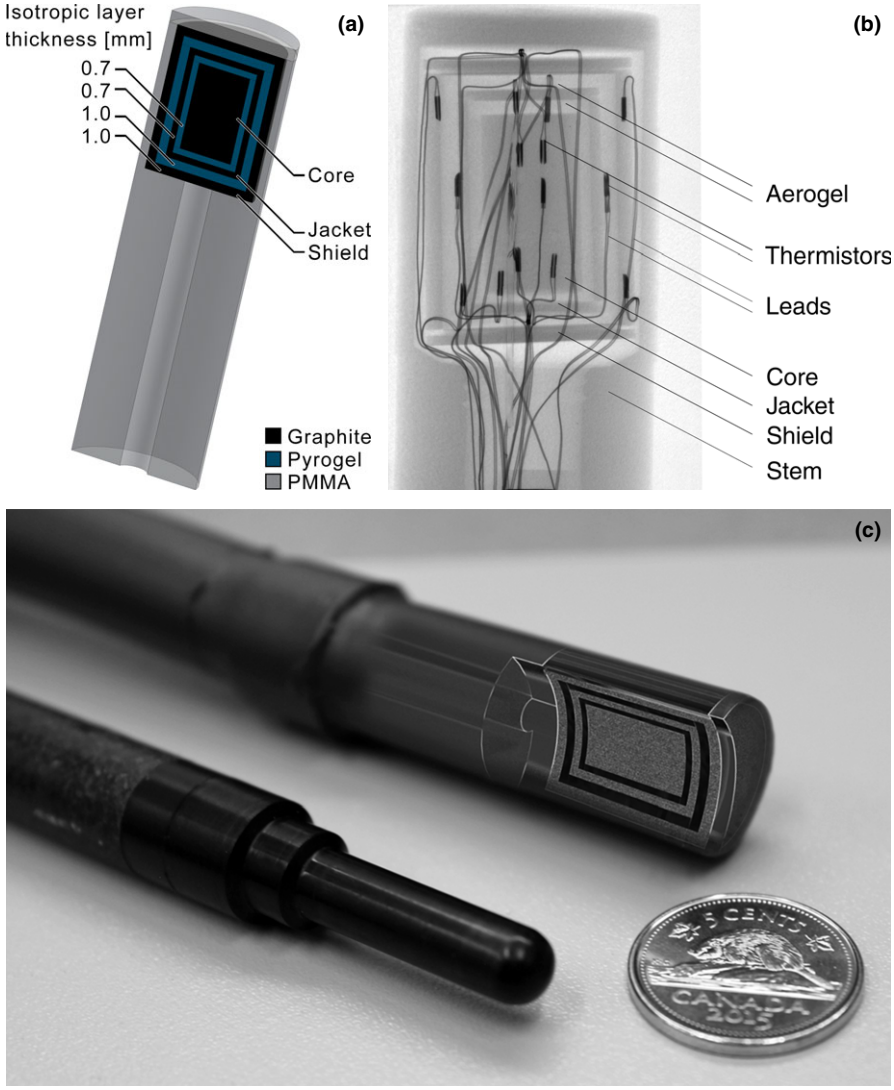

FIG. 1. (a) A cross-sectional schematic diagram of the Aerrow design, and (b) a digitally reconstructed radiograph of a micro-CT scan of the prototype calorimeter showing multiple embedded thermistors and leads. (c) The comparable size of the Aerrow to that of a Farmer — type ionization chamber is illustrated by the Exradin A12 positioned alongside the probe calorimeter (internal Aerrow structure is shown as a blended rendering) and a 5-cent coin (21 mm wide) for scale. [Color figure can be viewed at wileyonlinelibrary.com]

Each of the core, jacket and shield are fitted with negative temperature coefficient thermistors (H1744, US Sensor) with a nominal resistance of 10 kΩ at 25°C, which serve as either temperature sensors or Joule heaters. Each graphite component has one sensing thermistor, and three (core and jacket) or six (shield) thermistors connected in parallel for thermal regulation. They have been positioned in their respective graphite bodies to produce an axially — symmetric heating distribution. While fifteen thermistors far exceed the minimum required to operate the instrument, this quantity was selected to provide sufficient redundancy in the event of multiple connection failures in the prototype. The thermistor elements are approximately 0.13 mm thick, 0.28 mm wide, and 0.76 mm long, and are encapsulated in a 3.81 mm long, 0.43 mm diameter polyimide tube. An acrylic (PMMA) stem was fabricated to envelop and waterproof the calorimeter assembly for submerged dose measurements. It also serves as a rigid shell protecting the electrical connections from the physical strain of handling.

Like all graphite calorimeters, the core of the Aerrow consists of a certain amount of nongraphite materials (thermistors, epoxy, thermal insulation), herein referred to as impurities. The presence of impurities contributes to the perturbation of the absorbed dose in the graphite component of the core, both in the intuitive dosimetry sense (i.e., through radiation interactions), and thermally (e.g., different heat capacities contributing to heat transfer in the core). Table I lists the relevant material properties present in the prototype used in this work. Masses, m_i, were repeatedly measured using a high-precision balance (Type AJ100L, Mettler) at every stage of the assembly, whereas values for the specific heat capacities, $c_{p,i}$, were taken from literature.[33–35] A thermistor was dissected in order to separate and measure the individual component masses (nickel, polyimide, polyurethane nylon, transition metal oxide), which were found to be consistent with manufacturer-provided data to within about 0.2 mg. The relatively large fraction of mass contributed by the nickel (approximately 20% of the total core mass) represents the entirety of the 30 cm leads coming from the four core thermistors. Since the definition of the extent of the core is fuzzy, and the leads are a route for heat transfer to occur with the sensitive volume, we have opted to include all the mass over an arbitrary cut-off point.

2.B. Quasi-adiabatic operation

In general, graphite calorimeters can be operated in one of two independent modes to measure absorbed dose: quasi-adiabatic and isothermal (sometimes referred to as constant-temperature mode). In this work, the Aerrow was operated in both modes, the results of which were compared to one another as an initial self-consistency check. The quasi-adiabatic mode, as it has been implemented in this work, is not suitable for routine clinical application since it requires overnight stabilization much like a water calorimeter. Isothermal mode (see Section 2.C.) with its vastly reduced initial stabilization time, is expected to be the more practical of the two modes for clinical use.

In the quasi-adiabatic mode, no active thermal regulation is directly applied to the graphite; rather, the Aerrow is submerged in a temperature-controlled water phantom with a set point of 297.45 K. For this setup, the COMSOL-modeled time constant for heat conduction from the core to the surround is about 90 s. For reference, replacing the Pyrogel insulation with air gaps at atmospheric pressure (no mechanical supports included) reduces this time constant to about 40 s. Originally designed for use with McGill University's electron sealed water calorimeter (ESWcal),[36,37] the water phantom used in this work has been designed to regulate the water temperature drifts to within a few mK per hour. In this setup, the core, jacket, and shield temperatures rise when irradiated, causing a fractional resistance change of approximately 0.45 Ω/mK in the embedded thermistors. Changes in temperature are indirectly determined by measuring the response of a DC Wheatstone bridge circuit to resistance changes in the sensing thermistor. Two precision 10 kΩ resistors (model 1152, Burster) make up one arm of the bridge, while the sensing thermistor and an adjustable decade resistor box (Type 1408, Burster) make up the other. The bridge response voltage is measured (2182A nanovoltmeter, Keithey) and related back to temperature through separate calibrations of the thermistors (against a calibrated mercury thermometer traceable to national standards), and the bridge response.[38] Other calorimetry systems, such as the McGill ESWcal, use

TABLE I. Graphite and impurity contributions to the effective core mass and specific heat capacity of the Aerrow. The mass (m), absolute uncertainty (u), relative mass fraction of the core (w), and specific heat capacity (c_p) are given for each constituent material.

Core material	m_i (mg)	$u(m_i)$ (mg)	w (%)	$c_{p,i}$ (J kg^{-1} K^{-1})	$u(c_{p,i})$ (J kg^{-1} K^{-1})	$(c_{p,i}\cdot m_i)$ (J K^{-1})	$u(c_{p,i}\cdot m_i)$ (J K^{-1})
Graphite	539.2	0.1	71.50 ± 0.02	715	10	0.385	0.005
Nickel leads	159.2	0.2	21.11 ± 0.03	445	5	0.0708	0.0009
Polyimide tubing	0.8	0.2	0.11 ± 0.03	1110	20	0.0009	0.0002
Polyurethane nylon	12.0	0.2	1.59 ± 0.03	1650	50	0.0198	0.0007
Transition metal oxide	1.6	0.2	0.22 ± 0.03	600	200	0.0010	0.0003
Cyanoacrylate	5.5	0.5	0.73 ± 0.07	1420	50	0.0078	0.0008
Pyrogel® (50%–70% silica gel, 30%–50% polyacrylonitrile	35.9	0.5	4.76 ± 0.07	1080	20	0.0388	0.0009

an AC Wheatstone bridge in conjunction with a lock-in amplifier, which is generally less electrically noisy than an equivalent DC setup, but relatively more complex to construct.

The bridge response is calibrated by adjusting the decade resistor box setting by a known amount, typically 1 Ω, when the bridge is nominally balanced (i.e., the sensing thermistor resistance is equal to the decade resistor box setting). This bridge calibration procedure is performed in the absence of large drifts, regularly throughout the experiment. Collectively, these calibration results represent the change in bridge voltage per unit resistance change, $\Delta V_{1\ \Omega}$, as a function of balanced decade resistor box setting.

In the quasi-adiabatic mode, the Aerrow measures the mean absorbed dose in the core, D_{core}, based on its fundamental relation to the temperature rise, ΔT, and the effective specific heat capacity at constant pressure of the core (mass-weighted for graphite and impurities), $c_{p,\text{core}}$, as shown in Eq. (1).

$$D_{\text{core}} = \frac{\Delta E_{\text{rad}}}{m_{\text{core}}} = c_{p,\text{core}} \cdot \Delta T \cdot \prod k_i \tag{1}$$

For comparing operating modes, the product of the correction factors, $\prod k_i$, can be taken as simply the conductive heat transfer, k_c. The remaining corrections, the radiation field perturbation (k_p), the radiation dose nonuniformity over the extent of the graphite core (k_{dd}), and any radiation-induced heat defect (k_{hd}, arising either in the graphite or one or more of the impurities) are assumed to be independent of operating mode. With the exception k_{hd}, which has been assumed to be unity in this study, and k_c (see description below), all correction factors have been rolled into the absorbed dose-to-water conversion calculation (see Section 2.E.).

The acquired signal during a single quasi-adiabatic run consists of three distinct parts: the predrift, the irradiation period, and the postdrift (Fig. 2).[39] Prior to irradiation, a predrift signal is recorded to provide an initial state condition. During irradiation, the bridge signal resulting from the temperature rise at the core sensing thermistor is acquired. Following the irradiation, a postdrift signal is collected to compare against the initial slope of the predrift and provide a measure of the temperature rise. Due to the thermal insulation of the calorimeter box and the low thermal diffusivity of water, the pre- and postdrift signals are quasi-linear over the time scale of the measurement (heat transport within the system behaves nonlinearly, but can be accurately approximated as linear over sufficiently short time scales). The correction for heat loss due to conduction, k_c, is defined as the ratio of the temperature rise in the absence of conduction to the actual temperature rise, and is numerically simulated using a finite element method software package (COMSOL Multiphysics® v.4.2). Temperature gradients arise for two main reasons: (a) dose gradients induced by the nonuniform radiation field, and (b) the lower specific heat capacity of the graphite relative to the surrounding water, although in principle, all non-water materials contribute to this effect to varying degrees. The software can calculate time-dependent thermal distributions in a 3D model of the Aerrow (Fig. 3) by solving, in both time and space, the partial differential equation governing thermal conduction. The solving algorithm requires several input parameters including the physical and thermal properties of the involved materials, geometric boundary conditions, and the distribution of heat sources and sinks in space and time.

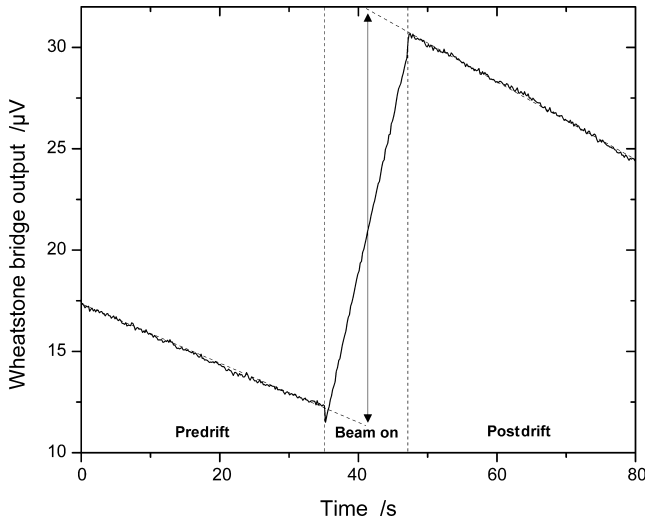

FIG. 2. Example of a 12 s quasi-adiabatic mode measurement acquired using the Aerrow in a 6 MV photon beam at a dose rate of approximately 7.5 Gy/min. During the beam-on period, the increasing bridge signal resulting from the temperature rise at the core sensing thermistor is acquired. This voltage offset (indicated by the vertical arrow) is directly proportional to the absorbed dose. The shifts exhibited at beam-on and off are electrical in nature, and are likely due to an unresolved ground loop. Though assumed to be always present, the effect is clearly visible in this run, but is indiscernible from the real signal in many others. While this effect has not yet been investigated, it may be introducing a systematic error in the dose determination, assuming the shifts do not cancel out.

2.C. Isothermal operation

The isothermal (or constant-temperature) mode of operation was first experimented on by Witzani et al.[40] and later further developed by Daures and Ostrowsky[41] of the LNE-LNHB to overcome the thermally dynamic nature of the quasi-adiabatic mode.[40,41] In this mode, each graphite component is subject to active thermal control such that a constant set point temperature is precisely maintained throughout operation. In this work, the core, jacket, and shield set points are 303.15 K, 302.95 K, and 301.65 K, respectively. Active control in the jacket and shield is done to prevent core signal perturbation due to thermal fluctuations in the surrounding environment, and removes the need for a thermally-controlled water phantom. Absorbed dose determination is based on an electrical substitution method. Conceptually, a constant temperature is maintained independently in each graphite body during the irradiation period by reducing the rate of electrical energy dissipated in the heating thermistors, $P_i(t)$, by an amount equal to the rate of energy deposited by the radiation. By subtracting the baseline power, $P_0(t)$, and integrating over the timespan, the total deposited energy, and hence the dose, can be derived. In this mode, *a priori* knowledge of the core

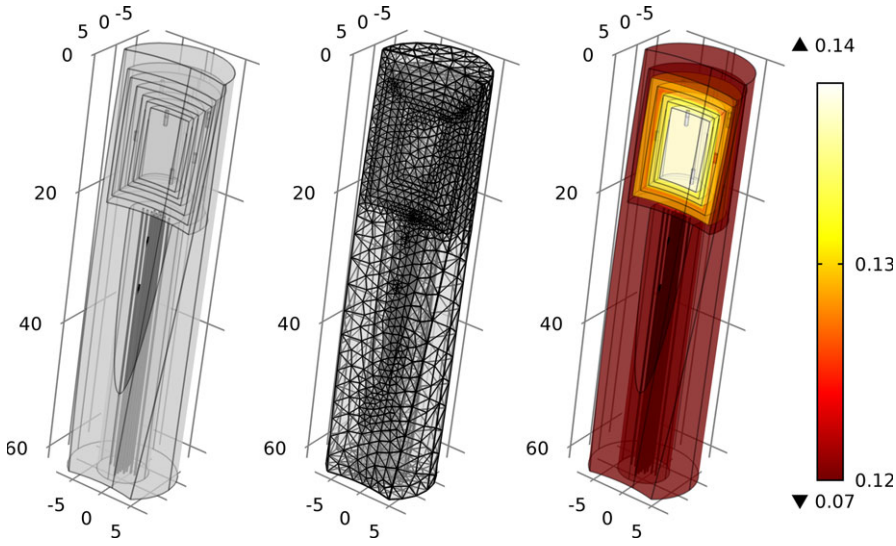

FIG. 3. Finite element analysis of the Aerrow using COMSOL Multiphysics®. (Left) Geometric 3D model with thermal property assignment of the involved materials, boundary conditions, and distribution of heat sources (based on physical estimates of the dose distribution) and sinks in space and in time are included as input parameters. (Centre) Discretization, or 'meshing', of the model into element domains over which the differential equations for heat conduction are solved by the software. (Right) Resulting radiation-induced time-dependent temperature distribution (baseline of 297.45 K subtracted; $0 < T < 0.15$ K) in the Aerrow at a time point, t, postirradiation. Please note that the depicted geometry is a modified version of the actual detector model and serves only to illustrate the finite element modeling flow. [Color figure can be viewed at wileyonlinelibrary.com]

mass, m_{core}, is required. In Equation 2, the product of the correction factors, $\prod k_i$, includes the mass impurity correction, k_{imp}, and the conductive heat transfer correction, k_c, which is assumed to be unity to within 0.1 % (see Section 3.E.). The expression for k_{imp} is shown in Eq. 3, and is also assumed to be unity to within 0.8% based on the approximation that, to first order, $\left(\frac{D_i}{D_{gr}}\right) \approx \left(\frac{\mu_{en}}{\rho}\right)^i_{gr}$, i and gr referring to impurity and graphite, respectively. This approximation assumes that the photon energy fluence is constant in both the graphite and the impurities, and that the range of the secondary electrons in the impurities is small compared to the dimensions of the impurities. The uncertainty figure of 0.8% comes from the k_{imp} value obtained when considering only nickel, which makes up about three quarters of the impurity content by mass. For a mean photon energy of 2 MeV and 3 MeV (approximating the effect in a 6 MV and 10 MV photon beam), the mass energy absorption ratios are 0.962 and 1.026, respectively. This translates to a k_{imp} of 0.995 and 1.008, hence the assigned 0.8% uncertainty. For reference, the continuous slowing down approximation (CSDA) range of 0.5 MeV electrons in graphite and nickel is 1.2 mm and 0.3 mm, respectively. While this assumption does not necessarily hold for the nickel wires when considering their diameter of 0.1 mm, it is assumed to be true when the detector is placed in a vertical orientation with respect to the beam and the predominantly forward-scattered electrons are more likely to travel along the long axis of the wires.

$$D_{\text{core}} = \frac{\Delta E_{\text{rad}}}{m_{\text{core}}} = \frac{\int_0^t (P_0 - P_i) \cdot dt}{m_{\text{core}}} \cdot \prod k_i \qquad (2)$$

$$k_{\text{imp}} = \frac{m_{\text{core}}}{m_{\text{gr}} + \sum_i m_i \cdot \left(\frac{D_i}{D_{gr}}\right)} \approx \frac{m_{gr} + \sum m_i}{m_{gr} + \sum_i m_i \cdot \left(\frac{\mu_{en}}{\rho}\right)^i_{gr}} \qquad (3)$$

As before, the variations in sensing thermistor resistance are measured by means of a precision DC Wheatstone bridge circuit. The voltage drop across each bridge is used as an input process variable, which is fed into a software-implemented PID controller (LabVIEW v.11.0, National Instruments) running at a sampling frequency of 6 Hz, with a set point of zero volts (i.e., a null and balanced bridge output). The controller regulates the temperature of a given graphite body by modulating the current output of a programmable DC power supply (PXI-4110, National Instruments) connected directly to the heating thermistor network embedded in that particular component. An accurate measure of the electrical power dissipated in the heating elements is continuously determined by measuring the voltage drops (PXI-4070, National Instruments) across the heating thermistor network, and serially connected precision resistor shunt (type 1152, Burster).[42]

As mentioned earlier, the advantage of isothermal operation is that it is considerably more time-efficient than quasi-adiabatic operation, since heater-driven temperatures are nearly static once equilibrium is reached (i.e., the final physical state of the system is virtually the same as the initial state). Also, no distinct electrical response calibration is required to derive the absorbed dose, since electrical power is continuously measured, with and without the presence of radiation.[41] That said, the response of the Aerrow to electrical power dissipation has been characterized in this work, not only to periodically verify the consistent operation of the isothermal mode, but also to study the effects of varying the rate and

duration of energy dissipation (analogous to the dose-rate dependence and response linearity). Emulating the energy deposition of a radiation field can be carried out electrically by manipulating the output parameters of the power supplies. The heating current output has two components: (a) the PID control, which is always active and maintains a constant temperature, and (b) an emulated beam components, which delivers a constant power equivalent to a radiation field specified by the user, and can be switched off/on. During a beam emulation, the PID controller will automatically respond to the sudden addition of extra current by reducing its own contribution in much the same way as it would in response to an irradiation. It is not dosimetrically equivalent, but by looking at the PID component of the current, we can investigate the response of the system, study different methods of analyzing the signal, and even tune the controller offline.

Like the quasi-adiabatic mode, the signal acquired during an isothermal run consists of a predrift, irradiation period, and postdrift. The principal difference is that rather than measuring the bridge voltage to derive the absorbed dose, the measurand is the electrical power dissipation in the core and the quantity of interest is the average absorbed dose rate to the core (Fig. 4). Prior to and following irradiation, a pre- and postdrift signal is recorded, respectively, to provide a baseline electrical power dissipation, $P_0(t)$ (in Fig. 4, points preceding 'A' and points proceeding 'D', respectively). During irradiation (points 'A' to 'C'), the decrease in the electrical power resulting from the addition of a radiation-induced energy contribution is acquired, with the transients (points 'A' to 'B' and 'C to D') being dropped from the analysis. The power deficit, $(P_0(t) - P_i(t))$, which is proportional to the average absorbed dose rate, is then determined by iteratively offsetting the irradiation signal following the first transient (points 'B' to 'C'; illustrated by vertically aligned gray copies of the signal) by a small, constant, positive power, dP. For each iteration, j, the signal without the transients (points 'A' to 'B' and points 'C' to 'D') is fit to a linear function and an adjusted R^2 is calculated. The power offset (sum of offsets, $\sum dP_j$) leading to a globally optimized fit (minimized adjusted R^2) is recorded as the average dose rate to the core. Timing information is measured based on the sharp transients observed in the signal that corresponds to when the beam is turned on and off (points 'A' and 'C'). Except for the transients, the signal is normally quasi-linear over the time scale of the run.

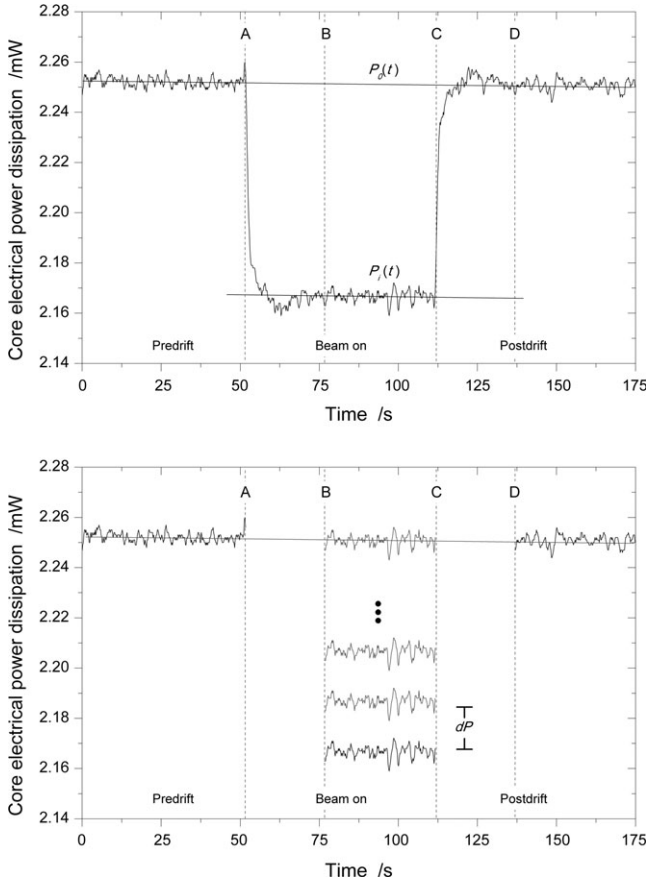

FIG. 4. (Top) example of a 60 s isothermal mode measurement acquired using the Aerrow in a 6 MV photon beam at a dose rate of approximately 7.5 Gy/min. Baseline power, $P_0(t)$, is fit from the points preceding 'A' and proceeding 'D'. (Bottom) the power deficit, $(P_0(t) - P_i(t))$, which is proportional to the average absorbed dose rate, is then determined by iteratively offsetting the irradiation portion (points 'B' to 'C'; illustrated by vertically aligned gray copies of the signal) of the acquired signal by a small, constant, positive power, dP, until the optimal (minimized adjusted R^2) linear fit is found. The average absorbed dose is equal to the sum of the offsets, $\sum_j dP_j$, divided by the mass of the core.

2.D. Reference dosimetry

The representation of uncertainties in this work follows that of the BIPM JCGM 100:2008 guide, and TG-51 notation will be used throughout.[12,13,43] As a first-stage evaluation of the Aerrow system, absorbed dose measurements were performed in a medical accelerator-based high-energy photon beam using the two independent calorimeter modes and compared against those acquired with a reference-class ionization chamber (Exradin A12, Standard Imaging Inc.) with a calibration traceable to the National Research Council of Canada (NRC) primary standard water calorimeter. This test was chosen based on the history of agreement that has been shown between other calorimeters and calibrated chambers of this type.[5] Calibrated in a reference ^{60}Co field, the uncertainty associated with the absorbed dose calibration coefficient, $N_{D,cw}^{60_{Co}}$, for the Exradin A12 was 0.5 %.[44] Dose to water in high-energy photons, as determined using the Aerrow, can be expressed analogously to TG-51, as shown in Eq. 4. In this expression, $f_{w,\text{core},60_{Co}}^{D_{\text{core}}\rightarrow D_w}$, is the dose conversion factor which converts dose to the graphite core in water to the dose to water in a ^{60}Co field (analogous to $N_{D,cw}^{60_{Co}}$), and k_Q is the quality conversion factor, which accounts for the change in the dose conversion factor between the beam quality of interest, Q, and ^{60}Co.

$$D_{w,Q} = D_{core,Q} \cdot f_{w,\text{core},60_{Co}}^{D_{\text{core}}\rightarrow D_w} \cdot k_Q \tag{4}$$

Graphite calorimetry was performed in a 6 MV photon beam ($\%dd(10)\times$ = 66.4) at a repetition rate setting of 1000 monitor unit (MU) per minute, a collimator field size setting

of 10 × 10 cm^2 at 100 cm from the source, a source to surface distance (SSD) of 107.6 cm, and at depth of 5 cm in 22°C water. The shallower reference depth and the extended SSD (normally 10 cm and 100 cm, respectively) represent distances practically achievable with the thermally regulated water phantom setup. A total of 25 quasi-adiabatic calorimetry measurements were performed by delivering irradiations of 200 MU (12 s nominally), equivalent to a dose of about 1.5 Gy at the position of the core. The beam-on time was kept relatively short to minimize the correction due to conductive heat loss, and 30 s of predrift and 30 s of postdrift data were collected for extrapolation and analysis.[45] Throughout the measurement set, 20 bridge calibrations were performed to quantify the voltage response to a 1 Ω change in resistance. Similarly, a total of 32 isothermal calorimetry measurements were performed by delivering irradiations of 1000 MU (60 s nominally), equivalent to a dose of about 7.6 Gy at the position of the core. In this operation mode, the beam-on time was kept relatively long, since preliminary electrical-based characterization of the Aerrow has suggested that the detector's accuracy is maximized at this time scale. While still a matter of investigation, the dependence of the accuracy upon exposure time may be related to one of the following: (a) the isothermal mode determines the absorbed dose by measuring the average dose rate, which may be more accurate for longer irradiations, and (b) the timing information provided by the acquisition software to calculate absorbed dose may introduce a systematic error given the finite sampling frequency that is minimized with increasing irradiation period. The different irradiation times used for quasi-adiabatic and isothermal may introduce a slight bias into the comparison (e.g., variable linac output at beam start-up affecting the two run lengths differently), however this issue was outweighed by practical considerations of the heat transfer and PID response time. For the isothermal mode measurements, 60 s of pre- and postdrift data were collected for analysis.

All chamber measurements were performed under the same conditions as the calorimeter measurements. An electrometer (6517A, Keithley) was used to read out the collected charge from irradiations of 200 MU (12 s nominally). The center of the chamber was positioned at the same depth that the calorimeter core had been positioned for the photon beam measurements. Water phantom temperature and air pressure were monitored using a mercury thermometer and mercury barometer (both traceable to national standards) to correct for environmental influences. Throughout the experiment, humidity remained in a range such that no correction was required. Correction for ion recombination and polarity effects were also applied per the AAPM's TG-51 protocol.[12]

2.E. Dose conversion

From the Aerrow's raw signal, a measure of the dose to graphite averaged over the core volume, D_{core}, is obtained for a given beam quality, Q. The quantity of interest is the absorbed dose to water, D_w, in the water phantom in the absence of the calorimeter, under otherwise identical conditions:

$$D_{w,Q} = \left(f_{w,\text{core},Q}^{D_{\text{core}}\rightarrow D_w}\right)_{MC} \cdot D_{\text{core},Q} \quad (5)$$

Where the dose conversion factor, $\left(f_{w,\text{core},Q}^{D_{\text{core}}\rightarrow D_w}\right)_{MC}$, is calculated using MC simulation, and implicitly includes the perturbative effects of the aerogel gaps and the impurities. In Eq. (5), $D_{w,Q}$ may be either evaluated at a point or volume averaged. The potential lack of electronic equilibrium caused by using this detector in a water phantom does not prevent the calculation of dose conversions, as this is not a prerequisite to determine the dose. In fact, Bouchard et al. drew several scenarios and gave a formal proof that charged particle equilibrium "cannot be practically achieved in a finite volume in external beam radiation therapy".[46] This method of MC calculation is analogous to the direct conversion method described by Wright et al. of the Australian Radiation Protection and Nuclear Safety Agency (ARPANSA) for their standard graphite calorimeter, or for that matter, the beam quality conversion factors for ionization chambers disseminated in dosimetry protocols.[47] In this work, a 3D model of the Aerrow inside a 30 × 30 × 30 cm^3 water phantom was modeled using the EGSnrc[48,49] Monte Carlo code system with the egs_chamber user-code of Wulff et al.[50] Geometries were modeled with the egs++ geometry package.[51] Cobalt-60 and Mohan photon spectra (4 MV, 6 MV, 10 MV, 15 MV, and 24 MV; $58.4\% < \%dd(10)\times < 86.8\%$) were used as simulation sources, which were set as 10 × 10 cm^2 parallel beams.[52] The global cut-off (ECUT) energies and production (PCUT) thresholds were set to 512 keV and 1 keV for electrons and photons, respectively. SMAX, ESTEPE, and XIMAX were set to 10^{10}, 0.25, and 0.5, respectively. The boundary cross algorithm was EXACT, the electron-step algorithm was PRESTA II, and all other transport parameters and cross-section options were kept to default. A minimum type A (sampling) uncertainty of 0.1% was sought out for each individual simulation by using a minimum of 10^9 primary histories. In addition to this type A uncertainty, there are systematic uncertainties associated with photon cross-sections and mean excitation energies that have not been considered in this work. These have been assigned a standard uncertainty of 0.35% to be consistent with other graphite calorimeters.[1] For variance reduction, a cross-section enhancement factor of 256, and a Russian roulette survival factor (N_R) of 512 with an associated ESAVE of 1 MeV were used. In cobalt-60 beams, the point of measurement (PoM) was taken at a depth of 5 cm on the central axis of the beam (i.e., the depth of calibration at calibration laboratories), which was centered on the phantom. In all other beams, the PoM was at a depth of 10 cm. $\left(f_{w,\text{core},Q}^{D_{\text{core}}\rightarrow D_w}\right)_{MC}$were calculated as the ratio of dose scored in a disk of water with a thickness of 0.025 cm and a radius of 1 cm centered on the PoM (as per the method described by Muir and Rogers[53]), to the dose in the graphite core volume, also centered about the PoM. For the reference dosimetry measurements (see Section 2.D), a separate dose conversion calculation was performed with the PoM situated at the experimental depth of 5 cm.

2.F. Isothermal characterization

A dosimetric characterization of the Aerrow's isothermal mode was carried out in medical accelerator-based high-energy photon beams (TrueBeam, Varian Medical Systems), at a depth of 2.5 cm, in a 17 cm thick, 30 × 30 cm^2 water-equivalent phantom (Solid Water®, Gammex RMI), under otherwise reference conditions. An Exradin A12, positioned at a depth of 7.1 cm in the same phantom, was used as an external monitoring chamber for the calorimetry measurements, which spanned the course of several evenings. All charge readings were corrected for deviations from the reference air density, as well as for polarity and ion recombination effects, in accordance with TG-51. The relative ion chamber readings were applied to the calorimeter datasets to account for the variation in accelerator output. Clinical reference dosimetry was performed for all beams using an Exradin A19 (SN/XAQ141084, Standard Imaging Inc.) and a SuperMAX electrometer (SN/P141014, Standard Imaging Inc.) with a calibration traceable to national standards. The photon qualities of interest in this study were a 6 MV, 6 MV FFF, 10 MV, 10 MV FFF, and 15 MV ($63.2\% < \%dd(10)\times < 76.3\%$) beam. Absolute dosimetry was performed with the Aerrow by delivering 60 s irradiations at the highest available repetition rate (600 to 2400 MU/min). The results of these measurements were directly compared to the chamber-derived doses.

In relative terms, the isothermal mode was evaluated for response linearity, dose-rate dependence, and angular dependence. The latter was carried out to investigate the possible effects of varying material thickness and lack of co-linearity of the graphite components due to the compressibility of the aerogel insulation. In each case, 60 s of pre- and postdrift data were collected for analysis. Linearity of the detector reading was evaluated in the 6 MV beam ($\%dd(10)\times = 66.3\%$) in the range of 0.8 Gy to 4.7 Gy by varying the number of MU (100 to 600; increments of 100) delivered at a fixed accelerator repetition rate of 600 MU/min. Dose-rate dependence was quantified, again in the 6 MV beam, in the range of 0.5 Gy/min to 5.4 Gy/min by maintaining a constant irradiation time of 60 s and varying the repetition rate from 60 MU/min to 600 MU/min. Angular dependence was characterized in the 6 MV beam by rotating the Aerrow about its major axis in increments of 90°. For this test, the position of the gantry and the direction of the beam delivery (0°) were kept constant.

3. RESULTS

3.A. Isothermal signal baselines

With the Aerrow embedded in a solid body phantom, the typical level of stability observed in the core electrical power dissipation was on the order of 1.5 μW/min, with an associated 1σ (standard deviation of the mean) signal variation of 1.2 μW. Given the effective mass of the core volume of this prototype, the latter amount of variation is equivalent to an absorbed dose rate of about 0.1 Gy/min. The two voltage measurements (thermistor heating network and precision shunt resistor voltages) from which this power is derived exhibit 1σ signal variations of about 1 mV each. In terms of control parameters, a negligible drift was observed in the bridge set point voltage (on the order of 1 nV/min) in comparison to the 1σ signal variations of about 90 nV. For this prototype design and operating conditions, a change in bridge voltage, ΔV, of 1 μV is approximately equivalent to a temperature change, ΔT, of 100 μK. Thus, the set point temperature in the core is maintained to within about 10 μK (1σ).

An example of an electrically emulated 8.5 Gy/min, 60 s irradiation is shown in Fig. 5 alongside an equivalent experimental measurement (labeled as 'actual beam') acquired under standard conditions in a water equivalent phantom. The user-initiated emulation was carried out by entering the desired dose rate and duration into the control software, which then drove the equivalent electrical parameters for each of the core, jacket, and shield based on mass information and the thermistor heating network voltages. In both cases, the signal variation is the same. There are, however, a few qualitative differences between the emulated and actual beam signals. Most notably, the emulated trace exhibits relatively large spikes in response to the "beam" being turned on and off. This feature is absent in the actual beam acquisition and is likely due to the abrupt addition and subsequent removal of the emulated beam current. Another difference is that a smaller relative rise in the postirradiation transient, as well as a quicker return to stability (appears as a less damped oscillation) is observed in the actual beam. This may be due to the difference in heating distributions; a radiation field will produce a relatively more uniform heating distribution than the emulated beam, which heats via quasi-point sources (thermistors) scattered throughout the graphite volumes. The

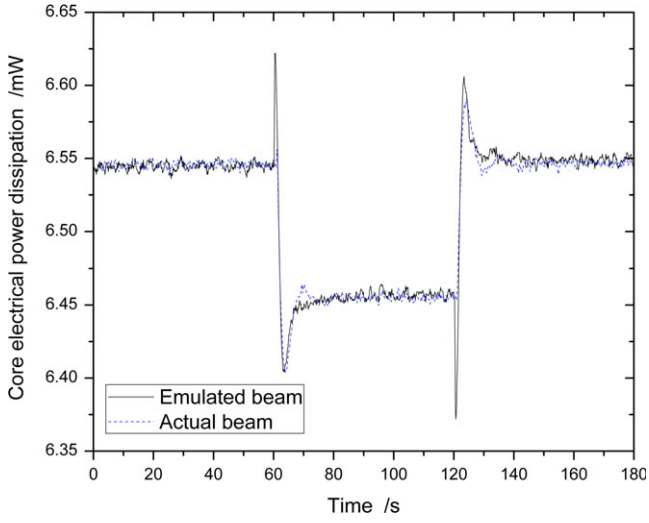

FIG. 5. Example of a 60 s isothermal mode measurement acquired using the Aerrow in a 6 MV photon beam overlaid on an equivalent electrically emulated irradiation (labeled 'Actual beam' and 'Emulated beam', respectively). Qualitative differences between the two signals include spikes in the emulated beam at the time of beam-on and beam off, as well as a smaller relative rise in the postirradiation transient and a quicker return to stability in the radiation-induced measurement. [Color figure can be viewed at wileyonlinelibrary.com]

emulation heating is expected to produce higher thermal gradients around these point sources, and thus the additional time required for these gradients to disperse in the graphite may be causing the observed difference in controller response. Dimensional analysis of the graphite's mass, specific heat capacity, thermal conductivity, and size suggests a thermal time constant of the order of a few tenths of a second to a few seconds, depending on the value of the conductivity, which is not known for the sample.

3.B. Dose conversion

MC-derived absorbed dose conversion factors, $(f^{D_{\text{core}}\rightarrow D_w}_{w,\text{core},Q})_{MC}$, were found to vary quasi-linearly between 1.117 ± 0.004 for ^{60}Co ($\%dd(10)\times$ = 58.4) and 1.136 ± 0.004 for the 24 MV Mohan spectrum ($\%dd(10)\times$ = 86.8). Figure 6 depicts $(f^{D_{\text{core}}\rightarrow D_w}_{w,\text{core},Q})_{MC}$ for the Aerrow normalized to ^{60}Co, as a function of beam quality.[54] For comparison, the beam quality conversion factor, k_Q, for an Exradin A12 ionization chamber is also shown in Fig. 6 as an example of a typical reference-class chamber.[13] In contrast to the ionization chamber's ~3.5% variation in k_Q across the range 58.4 < $\%dd(10)\times$ < 81.0, the Aerrow shows an equivalent ~1.5% variation.

3.C. Reference dosimetry comparison

As a first stage evaluation of the Aerrow, absorbed dose measurements were performed under reference conditions using the Aerrow's two independent modes (quasi-adiabatic and isothermal) and were directly compared to the dose derived from a calibrated reference-class ionization chamber (Exradin A12) in a 6 MV photon beam. A total of 25 quasi-adiabatic (200 MU; 12 s) and 32 isothermal measurements (1000 MU; 60 s) were acquired, a summary of which is provided in Table II. The repeatability (defined as 1σ) for both modes of operation in this experimental setup was 0.6%. For this beam quality, a $(f^{D_{\text{core}}\rightarrow D_w}_{w,\text{core},Q})_{MC}$ of 1.123 ± 0.004 was applied to the Aerrow measurements. For the quasi-adiabatic readings, a COMSOL-derived conductive heat transfer correction, k_c, of 1.002 ± 0.002 was additionally applied. The expressed uncertainty in the average temperature and energy columns represents the standard type A uncertainty for that measurement. The uncertainty in the absorbed dose-to-water columns reflects the combined standard uncertainty (k = 1) for that technique (see Section 3.E.). A combined standard uncertainty of 0.8% was assumed for the ionization chamber measurements, based on the best-case scenario as described in the TG-51 addendum and the 0.5 % uncertainty associated with $N^{60_{Co}}_{D,w}$.[13] The results of this study suggest self-consistency between the two Aerrow modes of operation. They also demonstrate statistical agreement between the doses measured using the quasi-adiabatic mode and that derived from the calibrated reference-class chamber. A small but statistically significant difference was found between the isothermal mode and the chamber measurements (2% lower) at the k = 1 level.

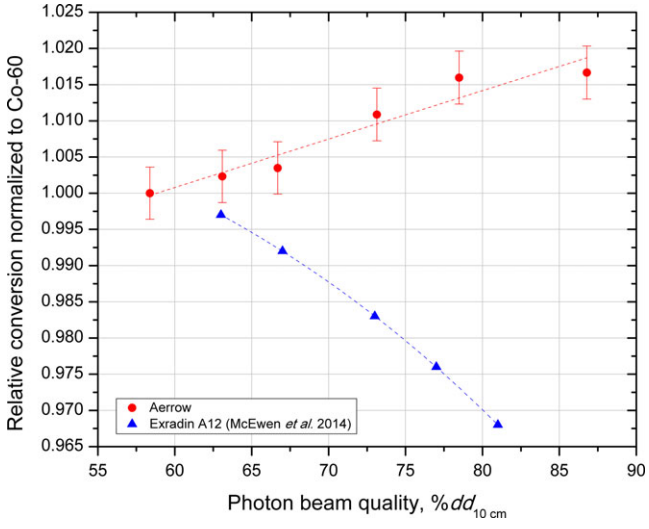

FIG. 6. The relative photon beam quality dependence for both the Aerrow (circles), and the Exradin A12 (triangles; cubic fit of the beam quality conversion factor from McEwen et al.[13]) in the therapeutic range. The Aerrow plot represents the normalized variation in the MC-calculated absorbed dose conversion factors, $(f^{D_{\text{core}}\rightarrow D_w}_{w,\text{core},Q})_{MC}$, which is primarily due to the beam quality dependence of the stopping power ratios. The Exradin A12 plot is representative of a typical reference-class ionization chamber. Both datasets are normalized to the beam quality of ^{60}Co ($\%dd(10)\times$ = 58.4). The apparent flattening of the Aerrow's conversion in the beam quality range greater than 80% is consistent with the behavior of the graphite to water stopping power ratio. [Color figure can be viewed at wileyonlinelibrary.com]

In a follow-up study, the Aerrow's isothermal mode was used to measure the absolute output of five high-energy photon beams at a depth of 10 cm, under reference conditions, in a water-equivalent phantom. These results, which are summarized in Fig. 7, were directly compared to the output measured using a calibrated reference-class chamber (Exradin A19). Overall, agreement was observed for all output measurements. As in Table II, the uncertainty in Fig. 7 reflects the combined standard uncertainty for the calorimeter (0.9%; k = 1) and ionization chamber (0.8%; k = 1) measurements. A minimum of five repeated measurements were performed for each beam quality. The repeatability of the isothermal measurements ranged between 0.4% (10 MV FFF; ~17 Gy/min) to 1.1% (6 MV; ~4 Gy/min). On average, the Aerrow's measured photon outputs were 0.1% smaller than those obtained with the chamber (range: −1.2% to 0.8%), though based on the distribution of data points, there does not appear to be any obvious systematic effect. The difference in the slopes of best fit in Fig. 7 (Exradin A19: 0.99 ± 0.01 cGy $\%^{-1}$; Aerrow: 1.08 ± 0.05 cGy $\%^{-1}$) could be indicative of some residual intrinsic energy dependency not being considered in this work (e.g., impurity correction).

3.D. Experimental characterization of the isothermal mode

Figures 8 and 9 show plots of the Aerrow's response linearity and dose-rate dependence, respectively. In the case of the former, a linear response with an adjusted R^2 value of 0.9998 (n = 30) is observed in the range of 80 cGy to

TABLE II. Summary of dose measurements performed using the two independent operating modes of the Aerrow in a 6 MV photon beam. Please note the differing number of MU's delivered in each case. The expressed uncertainty in the average temperature and energy columns represents the standard type A uncertainty for that measurement. The uncertainty in the absorbed dose-to-water columns reflects the combined standard uncertainty (k = 1) for that technique (see Section 3.E.). Percent difference noted in the last column is defined as [(Aerrow dose)−(TG-51 dose)]/(TG-51 dose) × 100%.

Aerrow mode of operation	Runs (#)	MU (#)	Avg. ΔT (mK)	Avg. ΔE (mJ)	Avg. D_w (cGy)	TG-51 D_w (cGy)[a]	Δ (%)
Quasi-adiabatic	25	200	1.878 ± 0.002	–	151.2 ± 1.4	152.5 ± 1.2	−1.2
Isothermal	32	1000	–	5.023 ± 0.006	747.2 ± 6.7	762.6 ± 6.1	−2.0

[a]The uncertainty expressed in this column (0.8%) is taken as a "best case" from McEwen et al.[13]

470 cGy. The five repeated measurements performed per data point exhibited a statistical variation (1σ, standard deviation of the mean) of 0.6% to 0.8% for all deliveries, except for the 100 MU (0.8 Gy) run, which varied by 1.4%. This relatively sharp increase in the spread of the data is due to the finite amount of time (~10 s) required for the temperature controllers to re-establish equilibrium during and after irradiation. In the case of the dose-rate dependence, no statistically significant effects are observed in the range of 0.5 Gy/min to 5.4 Gy/min. As seen in Fig. 9, the relative responses in this range all lie within ±0.8% of the average. Please note than the uncertainty bars in Fig. 9 represent the standard uncertainty of the mean measured signal, $\sigma/\sqrt{n}$, at a given dose rate. Like the linearity measurement sets, the statistical variation (1σ) for the dose rate data points down to 1.8 Gy/min ranged between 0.6 % and 1.0%, while an increase was seen at dose rates of 0.9 Gy/min (σ ~ 1.7 %) and 0.5 Gy/min (σ ~ 3.3 %). This behavior is attributed to a relative decrease in the signal to noise, which at 0.5 Gy/min, is equivalent to a dissipated power of about 6.5 μW in the core (normal 1σ signal variations are of the order of 1 μW). Finally, the angular dependence (gantry stationary and detector rotated) of the Aerrow's response is shown in Fig. 10 in increments of 90°. No statistically significant dependence is observed to within ±0.5% of the average taken across all angles. The uncertainty bars represent the standard uncertainty of the mean measured signal for a given angle.

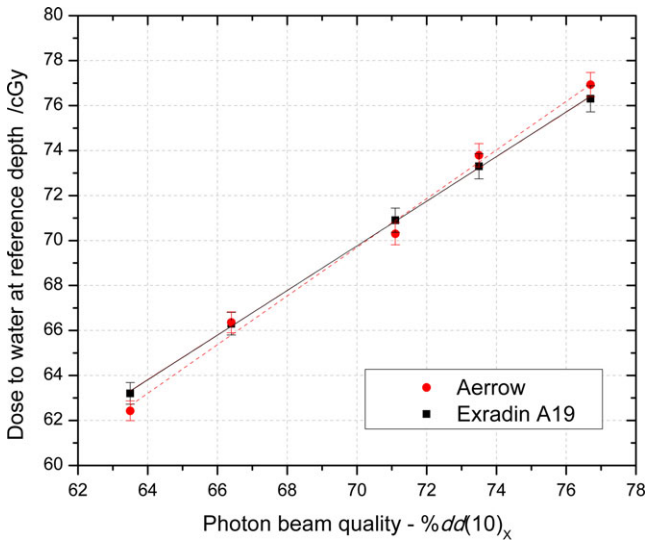

FIG. 7. A comparison of output measurements for five high-energy photon beam qualities (6 MV, 6 MV FFF, 10 MV, 10 MV FFF, and 15 MV) at a depth of 10 cm, as determined with the Aerrow operating in isothermal mode and a reference-class ionization chamber (Exradin A19). For all output measurements, the differences were not statistically significant. On average, the Aerrow measured an output 0.1% less (range: −1.2% to 0.8%) than that derived from the chamber readings. [Color figure can be viewed at wileyonlinelibrary.com]

3.E. Uncertainties

A breakdown of the estimated uncertainty budgets (in %), listing the largest contributing type A and B uncertainties associated with the determination of absorbed dose to water, is provided in Table III. The heat transfer correction used in the quasi-adiabatic mode measurements (assumed to be unity for isothermal), while likely near unity for this type of setup, has not been extensively studied with a proper sensitivity analysis. As such, this quantity has been assigned a standard uncertainty of 0.1–0.2%. The reproducibility represents the type A standard uncertainty for that type of measurement. Applicable to the quasi-adiabatic mode only, the bridge and thermistor calibrations reflect the uncertainty in the fits of their respective curves. Since the specific heat capacity of the

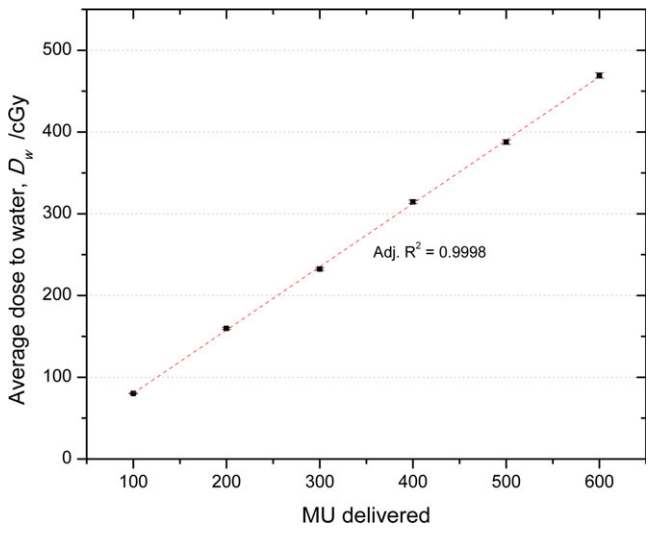

FIG. 8. The Aerrow's response linearity as experimentally determined in a 6 MV beam (%dd(10)× = 66.3%) in the range of 80 cGy to 470 cGy. Linearity of the detector reading was evaluated by varying the number of MU (100 to 600; increments of 100) delivered at a fixed accelerator repetition rate of 600 MU/min. [Color figure can be viewed at wileyonlinelibrary.com]

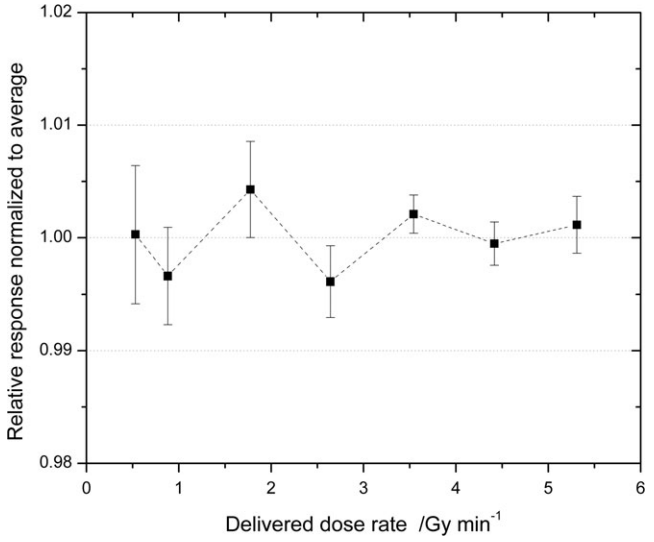

FIG. 9. The dose rate dependence of the Aerrow was quantified in a 6 MV beam in the range of 0.5 Gy/min to 5.4 Gy/min by maintaining a constant irradiation time of 60 s and varying the repetition rate from 60 MU/min to 600 MU/min. The relative response of the Aerrow is shown as normalized to the average response over all dose rates. No statistically significant effects in this range of dose rates are observed. The uncertainty bars in this plot are the standard uncertainties of the mean measured dose.

graphite used in the GPC's construction is unknown, a standard value with a rectangular uncertainty distribution of 715 ± 10 J kg^{-1} K^{-1} at 297.45 K was assigned based on experimentally determined values of pure samples found in the literature.[33-35] The positioning refers to the effect of the uncertainty in the GPC depth measurements, evaluated as 0.5 mm. Finally, the perturbation/dose conversion refers to the statistical and inherent (e.g., cross sections) uncertainty in the MC simulations used to calculate this quantity. Other sources of uncertainty not considered in this work include the accuracy of electrical power measurement, both in terms of acquisition and analysis, as well as other relatively minor effects, such as the radial nonuniformity correction.

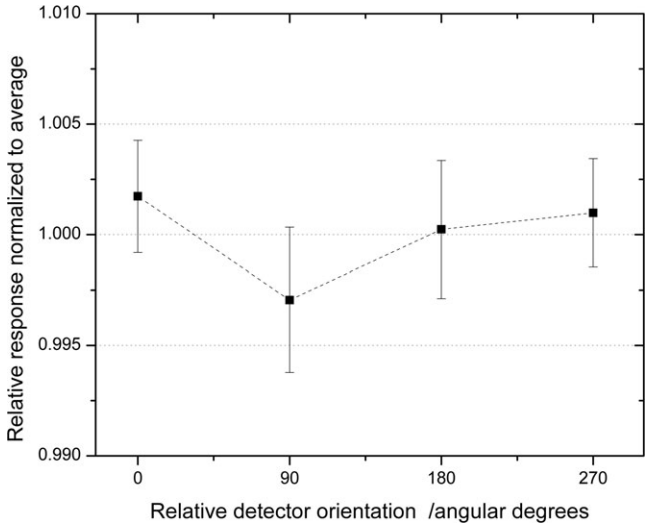

FIG. 10. The angular dependence of the Aerrow as measured in a 6 MV beam by rotating the detector about its major axis in increments of 90°. In this experiment, the gantry angle setting remained constant. The relative response of the Aerrow is shown as normalized to the average response over all detector orientations. No statistically significant dependence is observed to within ±0.5% of the average taken across all angles. The uncertainty bars represent the standard uncertainty of the mean measured signal for a given angle.

TABLE III. Estimated uncertainty budgets (in %) for the Aerrow's isothermal and quasi-adiabatic modes of operation in high-energy photon beams.

	Isothermal		Quasi-adiabatic	
Source of uncertainty	Type A [%]	Type B [%]	Type A [%]	Type B [%]
Heat transfer correction	—	0.1	—	0.2
Reproducibility	0.1	—	0.1	—
Bridge calibration	—	—	—	0.1
Thermistor calibration	—	—	—	0.2
Electrical power	—	0.2	—	—
Specific heat capacity	—	—	—	0.8
Mass impurity correction	—	0.8	—	—
Positioning	0.2	—	0.2	—
Dose perturbation/conversion	—	0.3	—	0.3
Other sources	—	0.2	—	0.2
Quadratic summation	0.2	0.9	0.2	0.9
Combined relative standard uncertainty on D_w	0.9		0.9	

4. DISCUSSION

Within combined uncertainties, the absorbed dose to water measured with the quasi-adiabatic mode in a 6 MV photon beam was found to agree with those derived from TG-51 using a calibrated reference-class ionization chamber. On the other hand, a statistically significant difference at the $k = 1$ level (2% lower) was measured between the absorbed dose to water obtained with the isothermal mode and the ionization chamber. Though the two Aerrow modes were used under different irradiation conditions, an intercomparison may be validly made when considering the results of the linearity and dose rate studies of the isothermal mode. The two operating modes agree within uncertainty, demonstrating self-consistency to within 0.8%. One possible reason for the lower relative dose measured in the isothermal mode could be an overestimation of the core mass. For instance, the thermistor leads extend to the readout electronics, and the components of the graphite-Pyrogel assembly are all in thermal contact, hence defining the extent of the core is inherently uncertain. The relatively lower dose obtained from the isothermal mode (about 0.8% lower than quasi-adiabatic) may be partly because it is based on an average dose-rate measurement and beam intensity from a medical linac is known to vary, particularly at the beginning of the irradiation where it can take a few seconds to establish the nominal intensity. Even if the transients are discarded during the analysis, intensity variations in the latter portion of the irradiation period will not be

captured. This is a distinct disadvantage of the isothermal mode as compared to the integrating quasi-adiabatic mode or ionization chambers. Nevertheless, the reference dosimetry results of this work demonstrate the feasibility of measuring absolute clinical photon absorbed doses to within a 2% accuracy using this type of probe-format calorimeter. Consequently, the issues surrounding traceability to absorbed dose-to-water primary standards must be carefully considered when proposing how such a device might be deployed clinically. On one hand, the Aerrow is potentially capable of circumventing all radiation standards to provide a truly independent check of clinical reference doses. On the other, it may serve as a transfer instrument, providing the clinic with a completely independent link to absorbed dose standards. The former may be attractive to some clinicians for whom an extra layer of dosimetric redundancy would serve to build confidence in the delivery accuracy, particularly when dealing with nonstandard reference fields. This scenario could become extremely problematic if the user were to elect to substitute, rather than supplement, the established calibration chain. The latter proposal would place the Aerrow in with a range of other dosimetry systems used for dose auditing, such as TLDs, OSLs, film, and alanine. However, it is not clear whether the introduction of on-site calorimetry would present any benefit, either in terms of cost or accuracy, to the auditing process. For instance, it has been shown that the beam quality dependence of the Aerrow is about half than of air-filled ionization chambers in the range $58.4 < \%dd(10)\times < 81.0$, but systems such as alanine exhibit a much lower dependence, about 0.6%, across the same range.[54] The main argument in support of the Aerrow as a transfer instrument is its inherit similarity to existing primary standard absorbed dose calorimeters; it stands to reason that a link made between a primary standard calorimeter and an absolute clinical reference dose would be more directly made through the Aerrow than through a dosimetry system operating on a completely different set of principles.

The Aerrow's two independent modes were evaluated by demonstrating self-consistency between quasi-adiabatic and isothermal operation, and by showing agreement to within 2% of an NRC-calibrated Exradin A12 chamber in a standard 6 MV photon beam. While the absolute accuracy of any primary technique (graphite calorimetry and water calorimetry-calibrated chamber) cannot be directly measured, showing agreement among independent methods helps to build confidence in the involved techniques.[3] Since the Exradin A12 was calibrated against a standard water calorimeter, this type of test can be considered an independent verification, since both calorimetry systems consist of different absorbing media and employ different approaches in determining correction factors. The level of agreement shown by both modes in this study suggests that there may remain systematic discrepancies in the absolute determination of dose, particularly for the isothermal mode. There are likely one or more minimally beam quality-dependent influencing quantities (e.g., the mass impurity effect) relevant in the therapeutic range, which are not being considered beyond a standard uncertainty assignment.[40] A reduction in the relative portion of non-graphite masses in the core (e.g., smaller and fewer thermistors, thinner leads, etc.) is expected to improve the accuracy in the determination of the core mass effective during irradiation. The level of uncertainty and accuracy achieved in this study is not yet on par with the performance expected of graphite calorimeters in the primary standards setting, which typically achieve a combined relative standard uncertainty on dose to water of 0.4 %. This is not an unexpected result, as compared to the standards laboratories, the Aerrow has followed a more pragmatic path of development, perhaps more in line with industry than science, and has been driven by the unique aim of clinical use on a mass scale. A rapid iterative cycle of prototyping and evaluation was chosen to demonstrate the feasibility and subsequently refine aspects of the Aerrow's design and operation, rather than building the most accurate instrument possible the first time around. This approach has led to some less-than-ideal conditions, most notably a relatively high impurity content in the core, but it has permitted the quick testing of new ideas. For example, a fewer number of smaller thermistors could have been used in this prototype, but this would have dramatically increased the complexity of the construction as well as the probability of failure due to failed electrical connections. With every new prototype come incremental improvements over previous ones, as well as a slew of new challenges to be addressed. The intent is to arrive at a viable concept design suitable for the clinic that combines ease-of-use as well as utility, and to gradually improve the performance (i.e., precision and accuracy) as experience is gained.

The implementation of the isothermal mode represents an important step toward the goal of developing a clinical-version of the Aerrow suitable for routine use. Compared to the quasi-adiabatic mode, the benefits of isothermal operation include a vastly decreased initial stabilization time (overall time ~10 mins) and the virtual elimination of intermeasurement delay. Further effort, however, is required to improve the repeatability, particularly for measurements involving dose rates of less than 2 Gy/min. This may be achieved through means of hardware (e.g., eliminating ground loops and crosstalk, improving the resolution of the current source, digitizing nearer to the detector, moving to AC bridges), software (e.g., signal averaging, alternative analysis technique) or both (e.g., analog or digital filtering). For instance, the sensitivity may be improved by adjusting the process control gains (specifically the proportional term) in response to a change in the dose rate; under conditions of zero or constant dose rate, the gains could be decreased, thus reducing the variation in the power signal, and conversely, they could be increased to more quickly respond to the change in the dose rate during beam-on and off. This is not an alternative analysis technique, but it may clean up the signal enough to apply other methods, such as frequency domain analysis.[55]

The same active thermal control systems developed to operate the Aerrow isothermally could also be used to intrinsically verify the response of the detector to electrical

energy.[1,41] Where dosimetry is concerned, this is a very powerful feature; aside from the benefit of not requiring radiation, electrically calibrating the Aerrow eliminates the need to know the effective specific heat capacity of the constituent graphite and thermistor assemblies, heat transfer correction, and thermistor temperature calibration. Such a feature could also be programmed to be fully automated and performed periodically when not in use. The practical impact of this functionality would be a dosimeter that could measure and notify a user of any potential drifts in its own response to energy. In general, the potential introduction of calorimetry as a mainstream device into the clinical setting is powerful, as this fundamental technique has formed the basis of absorbed dose standards in many countries for decades. Considered as the most direct means of measuring dose, a calorimetry-based local dose standard could play an important role in solving some of the major challenges of contemporary dosimetry. Investigations into the use of the Aerrow for MRgRT dosimetry, as well as plans to develop a further miniaturized Aerrow prototype suitable for small and composite field dosimetry are underway.

5. CONCLUSIONS

This work demonstrates the feasibility of using an ionization chamber-sized calorimeter as a practical means of measuring absolute dose to water in the radiotherapy clinic. In this study, the Aerrow was successfully used to quantify the absolute output of five high-energy photon beams (6 MV, 6 MV FFF, 10 MV, 10 MV FFF, and 15 MV; $63.2\% < \%dd(10)\times < 76.3\%$). Overall, doses to water were determined with a combined $k = 1$ uncertainty of 0.9% for the isothermal mode measurements, and 0.9% when operated quasi-adiabatically. In terms of relative characterization, the Aerrow exhibited a linear response, which was characterized by an adjusted R^2 value of 0.9998 in the region of 80 cGy to 470 cGy. No statistically significant dose-rate effects were observed in the range of 0.5 Gy/min to 5.4 Gy/min. Finally, the angular dependence of the Aerrow's response was found to be insignificant to within $\pm 0.5\%$ of the average taken across all angles.

ACKNOWLEDGMENTS

The efforts of Joe Larkin and Pavlos Papaconstadopoulos of the McGill University Health Centre, Greg Stanisz, Lynsie Thomason, and Ayelet Atkins of the Sunnybrook Research Institute, as well as David Marchington and Malcolm McEwen of the NRC-Canada are greatly appreciated. Allison Toltz of McGill University is credited with coining the name 'Aerrow'. This work has been supported in part by the CREATE Medical Physics Research Training Network grant of the Natural Sciences and Engineering Research Council (NSERC) (grant no. 432290), as well as NSERC grant RGPIN 298191 and 435608. J. Renaud is a recipient of a Canadian Institutes of Health Research doctoral scholarship.

[a]Author to whom correspondence should be addressed. Electronic mail: james.renaud@mail.mcgill.ca.

REFERENCES

1. Seuntjens J, Duane S. Photon absorbed dose standards. *Metrologia*. 2009;46:S39–S58.
2. Seuntjens JP, DuSautoy AR. Review of calorimeter-based absorbed dose to water standards. In: *Standards and Codes of Practice in Medical Radiation Dosimetry: Proc of an International Symposium IAEA-CN-96-3*. Vienna, Austria: International Atomic Energy Agency; 2003.
3. McEwen MR, DuSautoy AR. Primary standards of absorbed dose for electron beams. *Metrologia*. 2009;46:S59–S79.
4. Burns D. An analysis of existing data for Wair, Ic and the product of Wairsc, air. *Metrologia*. 2012;49:507–512.
5. BIPM (Bureau International des Poids et Mesures). Measurement of absorbed dose to water for Cobalt 60 – Key and supplementary comparisons, Ionizing Radiation, Section I (x and gamma rays, electrons). BIPM.RI(I)-K4. BIPM, Paris, France; 2015
6. Krauss A. The PTB water calorimeter for the absolute determination of absorbed dose to water in ^{60}Co radiation. *Metrologia*. 2006;43:259–272.
7. Ross CK, McEwen M, Klassen NV. Vessel designs and correction factors for water calorimetry. Workshop on Absorbed Dose and Air Kerma Primary Standards (Paris, France, 9-11 May 2007) (LNE, CEA-LIST-LNHB & BIPM).
8. Sarfehnia A, Stewart K, Seuntjens J. An absorbed dose to water standard for HDR ^{192}Ir brachytherapy sources based on water calorimetry: numerical and experimental proof-of-principle. *Med Phys*. 2007;34:4957–4961.
9. de Prez LA, de Pooter JA. The new NMi orthovoltage x-rays absorbed dose to water primary standard based on water calorimetry. *Phys Med Biol*. 2008;53:3531–3542.
10. Pinto M, Pimpinella M, Quini M, et al. A graphite calorimetry for absolute measurements of absorbed dose to water: application in medium-energy x-ray filtered beams. *Phys Med Biol*. 2016;61:1738–1764.
11. Harty PD, Lye JE, Ramanathan G, et al. Absolute x-ray dosimetry on a synchroton medical beam line with a graphite calorimeter. *Med Phys*. 2014;41:052101.
12. Almond R, Biggs PJ, Coursey BM, et al. AAPM's TG-51 protocol for clinical reference dosimetry of high-energy photon and electron beams. *Med Phys*. 1999;26:1847–1870.
13. McEwen M, DeWerd L, Ibbott G, et al. Addendum to the AAPM's TG-51 protocol for clinical reference dosimetry of high-energy photon beams. *Med Phys*. 2014;41:041501.
14. IAEA (International Atomic Energy Agency). Absorbed dose determination in external beam radiotherapy based on absorbed-dose-to-water standards: An international code of practice for dosimetry. Technical Report Series 398 (IAEA, Vienna, Austria, 2001).
15. Alfonso R, Andreo P, Capote R, et al. A new formalism for reference dosimetry of small and nonstandard fields. *Med Phys*. 2008;35:5179–5186.
16. O'Brien DJ, Roberts DA, Ibbott GS, Sawakuchi GO. Reference dosimetry in magnetic fields: formalism and ionization chamber correction factors. *Med Phys*. 2016;43:4915–4927.
17. Duane S, Aldehaybes M, Bailey M, Lee ND, Thomas CG, Palmans H. An absorbed dose calorimeter for IMRT dosimetry. *Metrologia*. 2012;49:S168–S173.
18. Daures J, Ostrowsky A, Rapp B. Small section graphite calorimeter (GR-10) at LNE-LNHB for measurements in small beams for IMRT. *Metrologia*. 2012;49:S174–S178.
19. Dufreneix S, Ostrowsky A, Le Roy M, et al. Using a dose-area product for absolute measurements in small fields: a feasibility study. *Phys Med Biol*. 2016;61:650–662.
20. de Prez L, de Pooter J, Jansen B, Aalbers T. A water calorimeter for on-site absorbed dose to water calibrations in ^{60}Co and MV-photon beams including MRI incorporated treatment equipment. *Phys Med Biol*. 2016;61:5051–5076.
21. Renaud J, Rossomme S, Sarfehnia A, et al. Development and application of a water calorimeter for the absolute dosimetry of short-range particle beams. *Phys Med Biol*. 2016;61:6602–6619.

22. Palmans H, Thomas R, Simon M, et al. A small-body portable graphite calorimeter for dosimetry in low-energy clinical proton beams. *Phys Med Biol*. 2004;49:3737–3749.
23. McEwen MR, Duane S. A portable calorimeter for measuring absorbed dose in the radiotherapy clinic. *Phys Med Biol*. 2000;45:3675–3691.
24. Renaud J, Marchington D, Seuntjens J, Sarfehnia A. Development of a graphite probe calorimeter for absolute clinical dosimetry. *Med Phys*. 2013;40:020701.
25. Sundara Rao IS, Naik SB. Graphite calorimeter in water phantom and calibration of ionization chambers in dose to water for ^{60}Co gamma radiation. *Med Phys*. 1980;7:196–201.
26. Berlyand VA, Bregadze YI. Portable calorimeter for measuring absorbed doses of x-rays and electrons from accelerators. *Meas Tech*. 1991;34:1179–1184.
27. Morishita Y, Kato M, Takata N, Kurosawa T, Tanaka T, Saito N. A standard for absorbed dose rate to water in a ^{60}Co field using a graphite calorimeter at the national metrology institute of Japan. *Radiat Prot Dosim*. 2012;154:1–9.
28. Guerra AS, Loreti S, Pimpinella M, et al. A standard graphite calorimeter for dosimetry in brachytherapy with high dose rate ^{192}Ir sources. *Metrologia*. 2012;49:S179–S183.
29. DuSautoy AR. The UK primary standard calorimeter for photon-beam absorbed dose measurements. *Phys Med Biol*. 1996;41:137–151.
30. Owen B, DuSautoy AR. Correction for the effect of the gaps around the core of an absorbed dose graphite calorimeter in high energy photon radiation. *Phys Med Biol*. 1991;36:1699–1704.
31. Hofmeester GH. Calorimetric determination of absorbed dose in water for 1 – 25 MeV x-rays*Biomedical dosimetry: Physical aspects, instrumentation, calibration* (*Paris, France, 27-31 Oct 1980*) (IAEA & WHO, IAEA-SM-249/56, 235-259).
32. McEwen MR, Duane S. Portable graphite calorimeter for measuring absorbed dose in the radiotherapy clinic. Standards and Codes of Practice in Medical Radiation Dosimetry (Vienna, Austria, 25-28 Nov 2002) (IAEA, IAEA-CN-96/9P, 115-121).
33. Heat capacity of the elements at 25°C. In: Lide DR, ed. *CRC Handbook of Chemistry and Physics*, 89th edn (Internet Version 2009). Boca Raton, FL: CRC Press/Taylor and Francis; 2009: 4–127.
34. Picard S, Burns DT, Roger P. Determination of the specific heat capacity of a graphite sample using absolute and differential methods. *Metrologia*. 2007;44:294–302.
35. Williams AJ, Burns DT, McEwen MR. Measurement of the specific heat capacity of the electron-beam graphite calorimeter. Rep. RSA(EXT) 40, National Physical Laboratory, Teddington, UK; 1993.
36. Stewart K, Klassen N, Ross C, Seuntjens J. Design and testing of a new sealed water calorimeter for electron beams. *Med Phys*. 2005;32:2419.
37. Renaud J, Sarfehnia A, Marchant K, McEwen M, Ross C, Seuntjens J. Direct measurement of electron beam quality conversion factors using water calorimetry. *Med Phys*. 2015;42:6357–6368.
38. Stewart KJ. The development of new devices for accurate radiation dose measurement: A guarded liquid ionization chamber and an electron sealed water calorimeter. Ph.D. thesis, McGill University, Montreal; 2007.
39. Domen SR, Lamperti PJ. A heat-loss-compensated calorimeter: theory, design, and performance. *J Res Natl Bur Stand A Phys Chem*. 1974;78A:595–610.
40. Witzani J, Duftschmid KE, Strachotinsky Ch, Leitner A. A graphite absorbed-dose calorimeter in the quasi-isothermal mode of operation. *Metrologia*. 1984;20:73–79.
41. Daures J, Ostrowsky A. New constant-temperature operating mode for graphite calorimeter at LNE-LNHB. *Phys Med Biol*. 2005;50:4035–4052.
42. Renaud J, Sarfehnia A, Seuntjens J. "On the practical use of calorimetry for routine absolute dosimetry in the radiotherapy clinic", World Congress on Medical Physics and Biomedical Engineering (Toronto, Canada, 7–12. *IFMBE Proceedings*. June 2015;51:667–670.
43. BIPM (Bureau International des Poids et Mesures). Evaluation of measurement data – Guide to the expression of uncertainty in measurement. JCGM 100:2008, First ed. (BIPM, Paris, France, 2008).
44. McEwen MR, Ross CK. Direct calibration of ion chambers in linac electron beams. Proc. of Absorbed Dose and Air Kerma Primary Standards Workshop, LNHB. Paris, 9-11 May 2007. www.nucleide.org/ADAKPS_WS
45. Domen SR. Advances in calorimetry for radiation dosimetry. In: Kase KR, Bjärngard BE, Attix FH, eds. *The Dosimetry of Ionizing Radiation*, Vol. II. Orlando, FL: Academic Press Inc; 1987:245–320.
46. Bouchard H, Seuntjens J, Palmans H. On charged particle equilibrium violation in external photon fields. *Med Phys*. 2012;39:1473–1480.
47. Wright T, Lye JE, Ramanathan G, et al. Direct calibration in megavoltage photon beams using Monte Carlo conversion factor: validation and clinical implications. *Phys Med Biol*. 2015;60:883–904.
48. Kawrakow I, Rogers DWO. The EGSnrc code system: Monte Carlo simulation of electron and photon transport. NRC Technical Report No. PIRS-701 v4-2-2-5 (National Research Council of Canada, Ottawa, Canada, 2007).
49. Kawrakow I. Accurate condensed history Monte Carlo simulation of electron transport. I. EGSnrc, the new EGS4 version. *Med Phys*. 2000;27:485–498.
50. Wulff J, Zink K, Kawrakow I. Efficiency improvements for ion chamber calculations in high energy photon beams. *Med Phys*. 2008;35:1328–1336.
51. Kawrakow I. egspp: The EGSnrc C++ class library. NRC Technical Report No. PIRS-899 (National Research Council of Canada, Ottawa, Canada, 2005).
52. Mohan R, Chui C, Lidofsky L. Energy and angular distributions of photons of medical linear accelerators. *Med Phys*. 1985;12:592–597.
53. Muir BR, Rogers DWO. Monte Carlo calculations of k_Q, the beam quality conversion factor. *Med Phys*. 2010;37:5939–5950.
54. Zeng GG, McEwen MR, Rogers DWO, Klassen NV. An experimental and Monte Carlo investigation of the energy dependence of alanine/EPR dosimetry: I. Clinical x-ray beams. *Phys Med Biol*. 2004;49:257–270.
55. Tosh RE, Chen-Mayer HH. Frequency-domain characterization of heat conduction in sealed water calorimeters. *Nucl Instrum Methods Phys Res A*. 2007;580:594–597.